Design of narrow-band Compton scattering sources for nuclear resonance fluorescence

F. Albert,* S. G. Anderson, D. J. Gibson, R. A. Marsh, S. S. Wu, C. W. Siders, C. P. J. Barty, and F. V. Hartemann

Lawrence Livermore National Laboratory, NIF and Photon Science, 7000 East Avenue, Livermore, California 94550, USA

(Received 20 December 2010; published 13 May 2011)

The design of narrow-band Compton scattering sources for specific applications using nuclear resonance fluorescence (NRF) is presented. NRF lines are extremely narrow ($\Delta E/E \sim 10^{-6}$) and require spectrally narrow sources to be excited selectively and efficiently. This paper focuses on the theory of spectral broadening mechanisms involved during Compton scattering of laser photons from relativistic electron beams. It is shown that in addition to the electron beam emittance, energy spread, and the laser parameters, nonlinear processes during the laser-electron interaction can have a detrimental effect on the gamma-ray source bandwidth, including a newly identified weakly nonlinear phase shift accumulated over the effective interaction duration. Finally, a design taking these mechanisms into consideration is outlined.

DOI: 10.1103/PhysRevSTAB.14.050703 PACS numbers: 41.60.−m, 07.85.Fv, 52.38.Ph

I. INTRODUCTION

Nuclear resonance fluorescence (NRF) [1] is an isotope-specific process in which a nucleus, excited by gamma-rays, radiates high energy photons at a specific energy. This process has been well known for several decades, and has potential high impact applications in homeland security, nuclear waste assay, medical imaging, and stockpile surveillance, among other areas of interest. Although several successful experiments have demonstrated NRF detection with broadband bremsstrahlung gamma-ray sources [2], NRF lines are more efficiently detected when excited by narrow-band gamma-ray sources. Indeed, the effective width of these lines, $\Delta E/E$, is on the order of 10^{-6}. Currently, Compton scattering is the only physical process capable of producing a narrow bandwidth radiation (below 1%) at gamma-ray energies, with state-of-the-art accelerator and laser technologies. In Compton scattering sources, a short laser pulse and a relativistic electron beam collide to yield tunable, monochromatic, polarized gamma-ray photons. Several projects have recently utilized Compton scattering to conduct NRF experiments: Duke University [3], Japan [4], and Lawrence Livermore National Laboratory (LLNL) [5–7]. In particular, LLNL's Thomson-radiated extreme x-rays (T-REX) project demonstrated isotope-specific detection of low density materials behind heavier elements [5].

This paper presents, within the context of NRF-based applications, the theoretical and conceptual design of a narrow-band monoenergetic gamma-ray (MEGa-ray) source. Section I gives a brief overview of NRF and motivates the need for a narrow-band source; Sec. II highlights Compton scattering properties, via detailed modeling of spectral broadening mechanisms. In particular, weakly nonlinear effects are studied in the picosecond regime. Finally, Sec. III presents a conceptual design for the source as well as expected gamma-ray performance.

II. NUCLEAR RESONANCE FLUORESCENCE

A. Overview

NRF lines are characterized by a very narrow linewidth and a strong absorption cross section. For actinides such as uranium, the NRF linewidth is due to the intrinsic linewidth Γ_0 connecting the excited state to the ground state and to the Doppler width:

$$\Delta = E_R\left(\frac{kT_{\mathrm{eff}}}{Mc^2}\right)^{1/2}, \tag{1}$$

where E_R is the resonant energy (usually MeV), M is the mass of the nucleus, k is the Boltzmann constant, c is the speed of light, and T_{eff} is the effective temperature of the material. This model is valid as long as $\Gamma_0 + \Delta \gg 2kT_D$, where T_D is the Debye temperature. Because in most cases $\Gamma_0 \ll 1$ eV, the total width is just determined by the thermal motion of the atoms. Debye temperatures for actinides are usually in the range 100–200 K. Within this context, the NRF absorption cross section near the resonant energy is [3]

$$\sigma(E) = \pi^{3/2}\left(\frac{\lambda}{2\pi}\right)^2\left(\frac{2J_j+1}{2J_i+1}\right)\frac{\Gamma_0}{\Delta}\exp\left[-\left(\frac{E-E_R}{\Delta}\right)^2\right], \tag{2}$$

where J is the spin, i and j the ground and excited states respectively, and λ the radiation wavelength. Typically, strong M1 resonances at MeV energies are on the order of tens of meV wide with an absorption cross section around 10 barns.

*Corresponding author.
albert6@llnl.gov

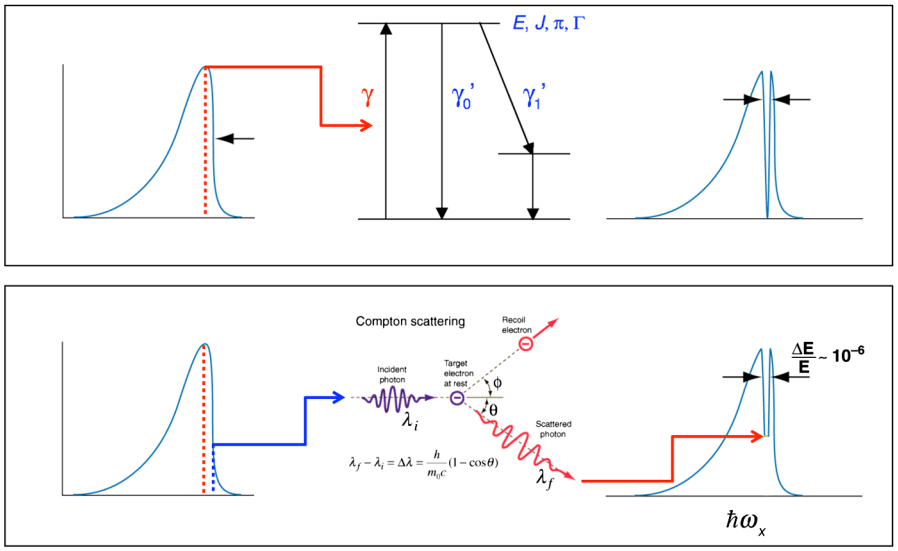

FIG. 1. (a) NRF and (b) notch refilling of NRF transmitted spectrum by elastic Compton scattering of higher energy photons.

B. NRF detection and notch refilling

In principle, given the large integrated cross section of NRF lines, a γ-ray beam transmitted through a small amount of an isotope of interest should exhibit a deep notch at the resonant frequency, because the NRF light is scattered into nearly 4π (dipole or quadrupole) solid angle. In practice, because the notch is very narrow, no detector currently has the resolution to detect such lines, which makes NRF detection very tedious.

A few years ago, Bertozzi and colleagues proposed a method that can ascertain the presence or absence of a given isotope with lower false positive and negative rates [8]. In this method, γ rays are transmitted through the material under interrogation to a reference sample containing the isotope of interest. If NRF is detected from the reference, one can conclude that the interrogated material did not contain the isotope. If no NRF is observed, either the resonant photons have been absorbed by the isotope in the interrogated sample or the material is optically too thick. In this case, the interrogated sample transmits a spectrum containing a notch at the resonant energy, as illustrated in Fig. 1(a). This method is very advantageous, and has been used successfully using bremsstrahlung sources [2,8], and Compton scattering sources [5].

However, it has been shown that the notch can be refilled by parasitic scattering processes [9], as illustrated in Fig. 1(b). Compton scattering of photons with energies larger than the resonant energy yield lower energy photons that can refill the notch and defeat the interrogation system. Although is has not been shown experimentally that notch refilling is an issue, and that bremsstrahlung sources work well for NRF detection because of their large photon yield, the photons with energies lower than the resonant energy will simply contribute to unwanted background and dose that MEGa-ray sources have the potential to reduce. Hence, the remainder of this paper focuses on the design of a narrow-band, precision MEGa-ray sources.

III. COMPTON SCATTERING PROPERTIES

A. Overview

The Compton formula can be derived from energy-momentum conservation, and expressed as follows:

$$u_\mu + \lambda k_\mu = v_\mu + \lambda q_\mu. \tag{3}$$

Here, u_μ and v_μ are the initial and scattered electron 4-velocities, while k_μ and q_μ are the incident and scattered 4-wave numbers, respectively. The 4-velocities are normalized, with $u_\mu u^\mu = v_\mu v^\mu = 1$, and the dispersion relation implies that $k_\mu k^\mu = q_\mu q^\mu = 0$. Hence, using these conditions in conjunction with Eq. (3) allows for the elimination of the scattered electron 4-velocity, and results in

$$u_\mu(k^\mu - q^\mu) = \lambda k_\mu q^\mu. \tag{4}$$

Equation (4) can be also written in a slightly different manner by introducing the incident and scattered light-cone variables [10], $\kappa = u_\mu k^\mu$, and $\lambda = u_\mu q^\mu$, respectively:

$$\kappa - \lambda = \lambda k_\mu q^\mu. \tag{5}$$

Finally, in regular units and 3-vector form: $u_\mu = (\gamma, \mathbf{u})$; $q_\mu = q(1, \mathbf{n})$, where $\mathbf{n}$ is the unit vector along the direction of observation; and $k_\mu = (k, \mathbf{k})$; this yields the well-known Compton formula:

$$\frac{q}{k} = \frac{\gamma - \mathbf{u}.(\mathbf{k}/k)}{\gamma - \mathbf{n}.\mathbf{u} + \lambda(k - \mathbf{n}.\mathbf{k})}. \tag{6}$$

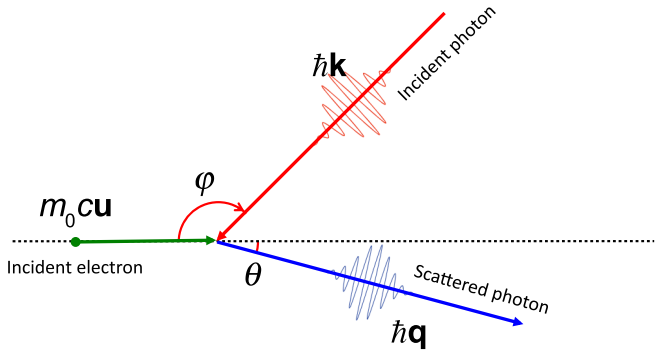

FIG. 2. Definition of the Compton scattering geometry for a plane wave interacting with a single electron.

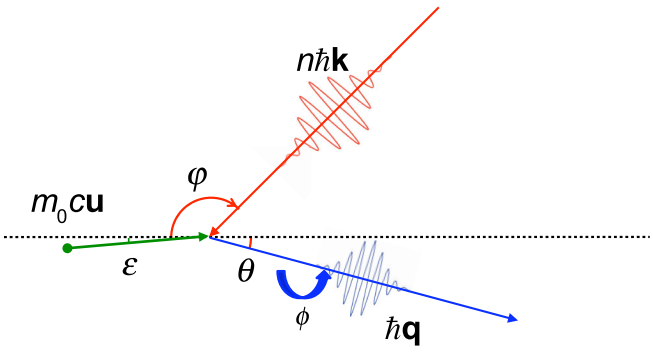

FIG. 3. Definition of the Compton scattering geometry in the case of an electron beam.

Here k is the wave number and $\gamma = 1/\sqrt{1 - v^2/c^2}$ is the electron relativistic factor. This approach is valid in the linear single photon interaction regime; nonlinear effects are discussed in a later section. By expressing Eq. (6) in terms of the interaction geometry of Fig. 2, the Compton scattering formula becomes

$$\frac{q}{k} = \frac{\gamma - u\cos\varphi}{\gamma - u\cos\theta + \lambda\!\!\!^{-}k[1 - \cos(\theta + \varphi)]}, \tag{7}$$

where φ is the angle between the incident laser and electron and θ is the angle between the incident electron and scattered gamma-ray photon.

B. Spectral broadening mechanisms

For realistic laser-electron interactions, one has to take into account the electron phase space and the laser transverse dimensions. In the case of a weakly focused laser pulse (typical for Compton scattering sources), the coordinates of the wave vector (k_x, k_y, k_z) remain close to their initial values $(0, 0, k_0)$ [11]. The exact nonlinear plane-wave solution for the 4-velocity has been derived in earlier work [11–13]:

$$u_\mu = u^0_\mu + A_\mu - k_\mu \frac{A_\nu(A^\nu + 2u^\nu_0)}{2k_\nu u^\nu_0}, \tag{8}$$

where u^0_μ is the initial 4-velocity and A_μ is the laser 4-potential. By using the nonlinear 4-velocity in conjunction with Eq. (4), one obtains

$$\left(u^0_\mu + A_\mu - k_\mu \frac{A_\nu A^\nu + 2u^0_\nu A^\nu}{2u^0_\nu k^\nu}\right)(k^\mu - q^\mu) = \lambda\!\!\!^{-}k_\mu q^\mu, \tag{9}$$

which, after applying the Lorentz gauge condition $k_\mu A^\mu = 0$, and the dispersion relation in vacuum, $k_\mu k^\mu = 0$, simplifies to

$$u^0_\mu k^\mu - \left(u^0_\mu - \frac{k_\mu}{2u^0_\nu k^\nu}\langle A_\nu A^\nu\rangle\right)q^\mu = \lambda\!\!\!^{-}k_\mu q^\mu. \tag{10}$$

This new relation is a modified form of the Compton formula, now including the nonlinear ponderomotive force of the laser field. It is important to note that the general form of the laser potential is, for a linearly polarized plane wave, $[A_0 g(\phi)\cos(\phi), 0, 0]$, where ϕ is the phase and $g(\phi)$ the laser pulse envelope. Hence, nonlinear effects are a direct consequence of the inhomogeneous nature of the laser electrical field.

When referring to the geometry described in Fig. 3, Eq. (10) becomes

$$\frac{q}{k} = \frac{\gamma - u\cos(\epsilon + \varphi)}{\gamma - u\cos(\theta + \epsilon) + [1 - \cos(\varphi + \theta + \epsilon)][\frac{\langle -A_\mu A^\mu\rangle}{2[\gamma - u\cos(\varphi + \epsilon)]} + \lambda\!\!\!^{-}k]}. \tag{11}$$

Here the small angle ϵ is different for each electron and represents the emittance of the electron beam. Note also that $\langle -A_\mu A^\mu\rangle$ is the nonlinear radiation pressure. By looking at the variation of q as a function of all the parameters in Eq. (11), for on-axis observation ($\theta = 0$) one finds that

$$\Delta q/q \propto \Delta k/k, \tag{12}$$

$$\Delta q/q \propto -\tfrac{1}{4}\Delta\varphi^2, \tag{13}$$

$$\Delta q/q \propto 2\Delta\gamma/\gamma, \tag{14}$$

$$\Delta q/q \propto -\gamma^2\Delta\epsilon^2, \tag{15}$$

$$\Delta q/q \propto -\frac{\Delta A^2}{1+A^2}. \tag{16}$$

While the gamma-ray spectral width depends directly on the electron and laser energy spreads, it is also strongly affected by the electron beam emittance because of the γ^2 factor. This provides a quick overview of the various sources of spectral broadening in a Compton scattering light source. Note that the negative variations are asymmetric broadening toward lower photon energies.

C. Klein-Nishina formalism

The Compton formula derived above provides a good approximation for the on-axis spectrum and within small angles ($\ll 1/\gamma$) of radiation. In general, one has to take into account the differential cross section to derive the source brightness. In Compton scattering, the total number of photons scattered by an electron distribution is given by

$$N = \int_{R^4} \sigma j_\mu \Phi^\mu d^4x, \tag{17}$$

where $j_\mu = n_e \frac{u_\mu}{\gamma}$ is the 4-current density and $\Phi_\mu = n_\lambda \frac{k_\mu}{k}$ the 4-photon flux. n_e and n_λ are the electron and photon density, respectively. Then

$$N = \int_{R^4} \sigma n_e n_\lambda \frac{u_\mu k^\mu}{\lambda k} d^4x. \tag{18}$$

In the case of a single electron, where $n_e = \delta[\mathbf{x}(\tau) - \mathbf{x}]$, the integral over space yields

$$N = \int_{-\infty}^{+\infty} \sigma \frac{\kappa}{\lambda k} n_\lambda[x_\mu(\tau)] c dt. \tag{19}$$

By differentiating the above equation, the number of photons scattered per unit frequency and solid angle is derived, assuming that in the case of an uncorrelated incident photon phase space, corresponding to the Fourier transform limit, the phase-space density takes the form of a product, $(d^3n_\lambda)/(d^3k) = n_\lambda(x_\mu)\tilde{n}_\lambda(k_\nu)$:

$$\frac{d^2N}{dqd\Omega} = \int_{-\infty}^{+\infty} \tilde{n}_\lambda(k)\delta(q-q_0) \int_{-\infty}^{+\infty} \frac{d\sigma}{d\Omega} \times \frac{\kappa}{\gamma k} n_\lambda[x_\mu(\tau)] c dt dk. \tag{20}$$

The quantity $d\sigma/d\Omega$ is the differential cross section. Here we use the expression as derived by Bhatt *et al.* [14], with the spin-independent part only:

$$\frac{d\sigma}{d\Omega} = \frac{1}{2}(\alpha \lambda\!\!\!^{-}_c)^2 \left(\frac{q}{\kappa}\right)^2 \left[\frac{1}{2}\left(\frac{\kappa}{\lambda} + \frac{\lambda}{\kappa}\right) - 1 + 2\left(\epsilon_\mu \pi^\mu - \frac{(\epsilon_\mu u^\mu)(\pi_\nu v^\nu)}{\kappa \lambda\!\!\!^{-}_c} + \frac{(\epsilon_\mu v^\mu)(\pi_\nu u^\nu)}{\lambda \lambda\!\!\!^{-}_c}\right)^2\right], \tag{21}$$

where α is the fine structure constant, $\epsilon_\mu = (0, 1, 0, 0)$ corresponds to a linearly polarized incident radiation, and π_μ is the scattered 4-polarization. $v_\mu = u_\mu + \lambda\!\!\!^{-}_c(k_\mu - q_\mu)$ is the 4-velocity after the scattering event. If we use the Compton formula in the Dirac delta function of Eq. (20), it yields to a pole in incident wave number:

$$k_p = \frac{q(\gamma - \mathbf{u}.\mathbf{n})}{\gamma - \mathbf{u}.\mathbf{m} - \lambda\!\!\!^{-} q(1 - \mathbf{m}.\mathbf{n})}, \tag{22}$$

where $\mathbf{m} = \mathbf{k}/k$ and $\mathbf{n} = \mathbf{q}/q$. With this solution, the integral over k is performed:

$$\frac{d^2N}{dqd\Omega} = \frac{d\sigma}{d\Omega}\frac{\kappa}{\gamma k}\left[\frac{\tilde{n}_\lambda(k)}{|dq_0/dk|}\right]_{k=k_p} \int_{-\infty}^{+\infty} n_\lambda[x_\mu(\tau)] c dt. \tag{23}$$

For a Gaussian laser pulse, the photon density in the Fourier domain is

$$\tilde{n}_\lambda = \frac{\exp[-(\frac{k-k_0}{\Delta k})^2]}{\sqrt{\pi}\Delta k}, \tag{24}$$

and the incident photon density can be modeled analytically within the paraxial approximation, and in the case of a cylindrical focus:

$$n_\lambda(\mathbf{x}, t) = \frac{N_\lambda}{\sqrt{\pi/2^3} w_0^2 c\Delta t} \frac{1}{1 + (z/z_0)^2} \times \exp\left[-2\left(\frac{t - z/c}{\Delta t}\right)^2 - 2\frac{r^2}{w_0^2[1 + (z/z_0)^2]}\right], \tag{25}$$

where N_λ is the total number of photons in the laser pulse, Δt the pulse duration, w_0 the $1/e^2$ focal radius, and $z_0 = \pi w_0^2/\lambda_0$ is the Rayleigh range. To evaluate the integral in (23), we replace the spatial coordinates by the ballistic electron trajectory:

$$\begin{aligned} x(t) &= x_0 + \frac{u_x}{\gamma} ct, \qquad & y(t) &= y_0 + \frac{u_y}{\gamma} ct, \\ z(t) &= z_0 + \frac{u_z}{\gamma} ct, \qquad & r^2(t) &= x^2(t) + y^2(t), \end{aligned} \tag{26}$$

where we can divide x, y and r by w_0 and z and ct by z_0 to obtain the normalized quantities $\bar{x}$, $\bar{y}$, $\bar{z}$, $\bar{r}$, and $\bar{t}$. One finally obtains the expression

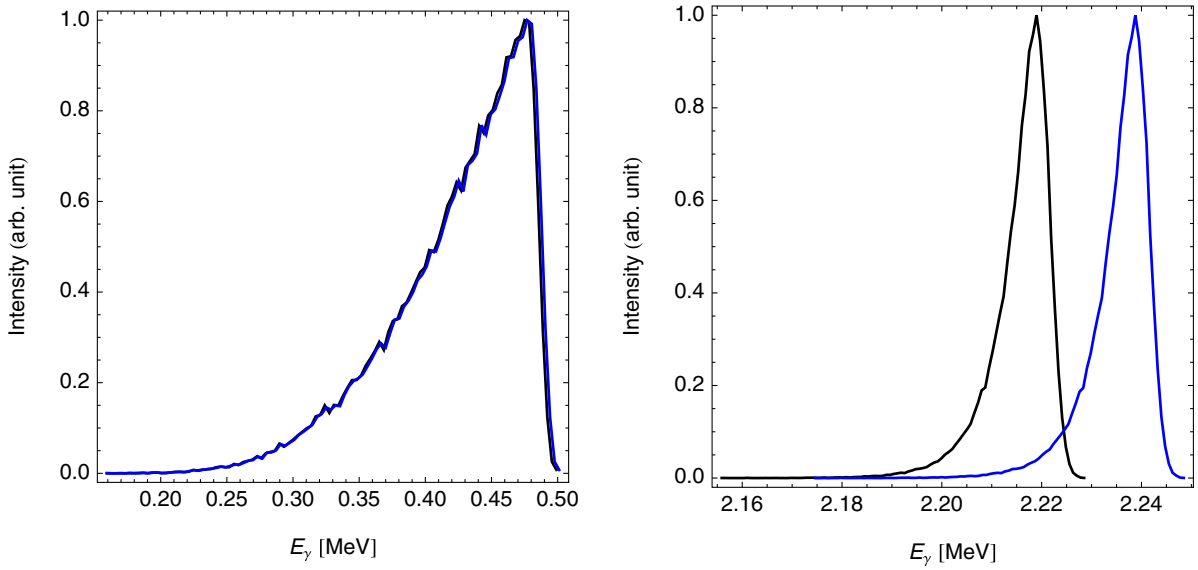

FIG. 4. Gamma-ray spectra in the case of Compton scattering (black) and Thomson scattering (blue). Left: T-REX source parameters (laser: 20 ps FWHM pulse duration, 532 nm wavelength, 34 μm rms spot size, 150 mJ; electron beam: 116 MeV, 40 μm rms spot size, 20 ps FWHM bunch length, 0.5 nC beam charge, 6 mm mrad normalized emittance). Right: future MEGa-ray source parameters (laser 10 ps FWHM pulse duration, 532 nm wavelength, 12 μm rms spot size, 150 mJ; electron beam: 250 MeV, 15 μm rms spot size, 10 ps FWHM bunch length, 0.25 nC beam charge, 1 mm mrad normalized emittance).

$$\frac{d^2N}{d\Omega dq} = \frac{1}{\sqrt{\pi}\Delta k}\left[\frac{d\sigma}{d\Omega}\frac{\kappa}{\gamma k}\frac{e^{-(k-k_0)^2/\Delta k^2}}{|\partial_k q_c(k)|}\right]_{k=k_p} \times \frac{N_\lambda}{\sqrt{\pi/2}^3 w_0^2 c\Delta t}\int_{-\infty}^{\infty}\frac{1}{1+\bar{z}^2} \times \exp\left[-2\left(\frac{z_0}{c\Delta t}\right)^2(\bar{t}-\bar{z})^2 - 2\frac{\bar{r}^2}{1+\bar{z}^2}\right]d\bar{t}. \quad (27)$$

Example on axis spectra for the previous source developed at LLNL [6,7] are shown in Fig. 4. It also shows the important of considering recoil in the case of narrow-band gamma-ray operation.

D. 1D weakly nonlinear effects

The Klein-Nishina formalism presented above is very good to model recoil, but does not take into account nonlinear effects. Within the context of laser-plasma and laser-electron interactions, nonlinear effects are neglected unless the normalized laser potential A approaches unity. $A = \sqrt{-A_\mu A^\mu}$ is most commonly described in practical units: $A = 8.5 \times 10^{-10}\ \lambda_0[\mu\text{m}]I^{1/2}[\text{W/cm}^2]$, where m_0 is the electron mass, c the speed of light, λ_0 the laser wavelength, and I the laser intensity. Typically, for current MEGa-ray sources, $A \simeq 0.1$ or less. We will show that, despite being in a regime where $A^2 \ll 1$, nonlinear effects can strongly increase the width of the gamma-ray spectra.

Here, nonlinear spectra can be calculated from the electron trajectories by using the covariant radiation formula that describes the number of photons scattered per unit frequency and solid angle:

$$\frac{d^2N}{dqd\Omega} = \frac{\alpha}{4\pi^2}q\left|\int_{-\infty}^{+\infty}\pi_\mu u^\mu e^{-iq_\nu x^\nu}d\tau\right|^2. \quad (28)$$

α is the fine structure constant; π_μ and q_μ are the 4-polarization and the 4-wave number of the scattered radiation; $x_\mu(\tau)$ is the electron 4-trajectory that is obtained by integrating the 4-velocity. For an incident plane wave, it is useful to use the electron phase, $\phi = k_\mu x^\mu$, as the independent variable. We also introduce the incident light-cone variable [10], defined by $\kappa = d\phi/d\tau = k_\mu \frac{dx_\mu}{d\tau} = k_\mu u^\mu$. By using Eq. (8), the Lorentz gauge $k_\mu A^\mu = 0$ and the dispersion relation $k_\mu k^\mu = 0$, κ is shown to be constant: $\kappa = k_\mu u_0^\mu$. Hence, $u_\mu(\tau) = \frac{1}{\kappa}u_\mu(\phi)$, $x^\nu = \int\frac{u^\nu}{\kappa}d\psi$ and Eq. (28) now reads

$$\frac{d^2N}{dqd\Omega} = \frac{\alpha}{4\pi^2}\frac{q}{\kappa^2}\left|\pi_\mu\int_{-\infty}^{+\infty}u^\mu(\phi)e^{-iq_\nu\int(u^\nu/\kappa)d\psi}d\phi\right|^2. \quad (29)$$

To account for recoil, consider a monochromatic incident plane wave with vanishingly small amplitude $a_\mu A_0 e^{i\phi}$, where $a_\mu a^\mu = -1$; adding the quantum correction $\lambda\!\!\!^{-}k_\mu$ to the 4-velocity yields $u_\mu = \kappa dx_\mu/d\phi = u_\mu^0 + A_\mu - k_\mu[(A_\nu u_0^\nu)/(k_\nu u_0^\nu)] + \lambda\!\!\!^{-}k_\mu$, which integrates to $x_\mu - x_\mu^0 = \kappa^{-1}(u_\mu^0 + \lambda\!\!\!^{-}k_\mu)\phi$. Here, $\lambda\!\!\!^{-} = \hbar/m_0c$ is the reduced Compton wavelength of the electron. Defining the incident 4-polarization in a covariant, gauge invariant manner [14],

as $\epsilon_\mu = \frac{1}{\sqrt{-A_\nu A^\nu}}\{A_\mu - k_\mu[(A_\nu u_0^\nu)/(k_\nu u_0^\nu)]\}$, the scattered radiation spectral density is

$$\frac{d^2N}{dqd\Omega} = \frac{\alpha}{4\pi^2}\frac{q}{\kappa^2}A_0^2|e^{-iq_\nu x_0^\nu}|^2|\pi_\mu \epsilon^\mu|^2 \times \left|\int_{-\infty}^{+\infty} e^{i\phi[1-(\lambda+\lambda q_\nu k^\nu/\kappa)]}d\phi\right|^2. \quad (30)$$

Equation (30) contains the coherence factor [15], the dipole radiation pattern, and a Dirac delta function spectrum centered at a frequency satisfying the condition: $\kappa - \lambda = \lambda q_\mu k^\mu$, where $\lambda = q_\mu u_0^\mu$ is the scattered light-cone variable [10]. Importantly, this condition satisfies the Compton formula: considering energy-momentum conservation, we have $u_\mu^0 + \lambda k_\mu = \upsilon_\mu + \lambda q_\mu$, where υ_μ is the electron 4-velocity after the interaction. Since $\upsilon_\mu \upsilon^\mu = 1$, $[u_\mu^0 + \lambda(k_\mu - q_\mu)][u_0^\mu + \lambda(k^\mu - q^\mu)] = 1$, the sought after result is obtained using $u_\mu^0 u_0^\mu = 1$, $k_\mu k^\mu = 0$, and $q_\mu q^\mu = 0$. Moreover, in the classical limit where $\lambda \to 0$, the Thomson scattering formula is recovered.

Equation (29) can now be used to study nonlinear spectra. First, let the laser 4-potential be

$$A_\mu = A_0(a_\mu \sin\phi + \sigma b_\mu \cos\phi), \quad (31)$$

with $a_\mu a^\mu = b_\mu b^\mu = -1$ and $a_\mu b^\mu = a_\mu k^\mu = b_\mu k^\mu = 0$; $\sigma = 0, \pm 1$ correspond to linear or circular polarization states. In the case of a plane wave with an envelope, $g(\phi)$, it can be shown that for on-axis radiation, the linear transverse oscillations do not contribute to the radiation phase if the wave is counterpropagating with respect to the electron. The total phase is

$$\Phi = q_\mu(x^\mu - x_0^\mu) = \frac{\phi}{\kappa}(q_\mu u_0^\mu + \lambda q_\mu k^\mu) + \frac{q_\mu k^\mu}{2\kappa^2}A_0^2 \times \int g^2(\phi)(\sin^2\phi + \sigma^2\cos^2\phi)d\phi. \quad (32)$$

Furthermore, an exact analytical result can be obtained for a circularly polarized hyperbolic secant pulse, where $g(\phi) = \mathrm{sech}(\frac{\phi}{\Delta\phi})$:

$$\Phi - \frac{q_\mu}{\kappa}(u_0^\mu + \lambda k^\mu)\phi = \frac{q_\mu k^\mu}{2\kappa^2}A_0^2\int_{-\infty}^{\phi}\mathrm{sech}^2\left(\frac{\psi}{\Delta\phi}\right)d\psi = \frac{q_\mu k^\mu}{2\kappa^2}A_0^2\Delta\phi\left[1 + \tanh\left(\frac{\phi}{\Delta\phi}\right)\right], \quad (33)$$

which clearly shows the $A_0^2\Delta\phi$ scaling of the nonlinear phase. Choosing the interaction region so that $k_\mu = (k, 0, 0, k)$, $u_\mu = (\cosh\rho, 0, 0, -\sinh\rho)$, and $q_\mu = (q, 0, 0, -q)$, which corresponds to head-on collisions and on-axis observation, the radiation integral reads

$$\frac{d^2N}{dqd\Omega} = \frac{\alpha}{4\pi^2}\frac{\chi}{k}|A_0 e^{i\chi A_0^2\Delta\phi}| \times \left|\int_{-\infty}^{\infty}\frac{\mathbf{x}\sin\phi + y\cos\phi}{\cosh(\phi/\Delta\phi)} \times \exp\left\{i\chi\left[\phi(1+r) + A_0^2\Delta\phi\tanh\frac{\phi}{\Delta\phi}\right]\right\}d\phi\right|^2. \quad (34)(35)$$

Here, $\chi = qe^{2\rho}/k$ is the normalized Doppler-shifted (Thomson scattering) frequency, and $r = 2\lambda k e^\rho$ is the recoil. We note that for linear polarization, A_0^2 can be replaced by $\langle A_0^2\rangle = \frac{1}{2}A_0^2$. Two changes of variable lead to an analytically tractable integral [15]; first, let $x = e^{\phi/\Delta\phi}$; next, set $z = (x^2 - 1)/(x^2 + 1)$, to obtain

$$\frac{d^2N}{dqd\Omega} = \frac{\alpha}{4\pi^2}\frac{\chi}{k}\left|\int_{-1}^{+1}(1+z)^{-(1/2)-(i/2)\Delta\phi[\chi(1+r)\pm 1]}(1-z)^{-(1/2)+(i/2)\Delta\phi[\chi(1+r)\pm 1]}(\mathbf{y}\pm i\mathbf{x})e^{iA_0^2\Delta\phi\chi z}dz\right|^2 = \frac{\alpha}{2}\frac{\chi}{k}A_0^2\sum|L_{(i/2)\Delta\phi[\chi(1+r)\pm 1]-(1/2)}(2iA_0^2\Delta\phi\chi)|^2\mathrm{sech}^2\left\{\frac{\pi\Delta\phi}{2}[\chi(1+r)\pm 1]\right\}. \quad (36)$$

Here, $L_n(x)$ is the nth Laguerre polynomial [16]. Spectra for different values of $\Delta\phi$ and A are shown in Fig. 5. The downshifting due to radiation pressure is evident, and the number of spectral lines is equal to the nonlinear phase accumulated over the pulse, $A_0^2\Delta\phi[\lim_{\phi\to+\infty}\tanh(\phi/\Delta\phi)] - [\lim_{\phi\to-\infty}\tanh \times (\phi/\Delta\phi)] = 2A_0^2\Delta\phi$, divided by 2π. In addition, the amplitude of the main spectral line first scales quadratically with A_0, then reaches a maximum, and slowly decays, as the scattered energy is distributed over an increasing number of spectral lines. The underlying physics can be understood as follows: the inhomogeneous radiation pressure leads to a slow dephasing between the electron and the scattered radiation that accumulates over the entire interaction; if the nonlinear phase integral is large enough, interference effects result in discrete anharmonic lines. Alternatively, one can think of this process as a competition between the bandwidth of the laser and nonlinear dephasing: if the laser spectrum is narrow enough, one can resolve increasingly small nonlinear effects. Example

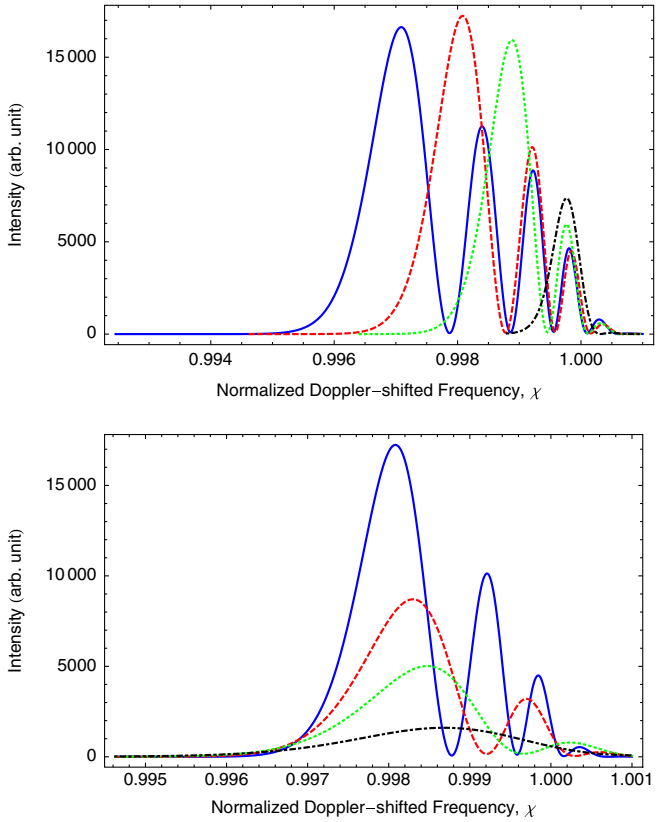

FIG. 5. Single electron spectra for $\gamma = 500$ and a laser wavelength of 532 nm. (a) Variation of $A = 0.06$ (solid blue curve), 0.05 (dashed red curve), 0.04 (dotted green curve), and 0.02 (dot-dashed black curve) for $\Delta\phi = 5000$ and (b) variation of $\Delta\phi = 5000$ (solid blue curve), 3000 (dashed red curve), 2000 (dotted green curve), 1000 (dot-dashed black curve) for $A = 0.05$.

spectra are shown in Fig. 5, for variations of A and $\Delta\phi$. Note that when $\Delta\phi$ decreases, not only the nonlinear features disappear but the gamma-ray spectrum broadens due to a broadening of the laser bandwidth.

E. 3D weakly nonlinear effects

To accurately simulate realistic interactions between a high brightness electron beam and a laser pulse, and study their influence on high-precision Compton scattering light sources, a fully 3D code is required. For long, narrow-band laser pulses, a direct approach, accounting for fine details in the correlated electron beam phase space, is computationally intensive. Instead, one can take advantage of the slow-varying pulse envelope, paraxial, and weakly nonlinear approximations to develop a local plane-wave model leading to analytical expressions for the electron 4-trajectory. The corresponding three small parameters are $\Delta\phi^{-1}$, $\epsilon = (k_0 w_0)^{-1}$, and A_0, respectively. For large Doppler upshifts, these conditions ensure that the particle excursions from ballistic trajectories are very small compared to all other scales characterizing the system. In turn, this allows the use of a local plane-wave model, where all dynamical variables become functions of ϕ: the six-dimensional input phase space specifies a ballistic trajectory for a given electron, $x^i_\mu(\phi) = x^{0i}_\mu + \phi(u^{0i}_\mu/\kappa_i)$; all other dynamical quantities are evaluated along this 4-trajectory.

A Fourier transform-limited Gaussian laser pulse and a six-dimensional uncorrelated Gaussian electron beam phase space are modeled here to provide a baseline example; the general method will be the object of another paper. The three-dimensional electromagnetic fields are generated from the vector $\mathbf{G}$, by taking $\mathbf{A} = \boldsymbol{\nabla} \times \mathbf{G}$, thus ensuring a divergence-free potential vector satisfying the Coulomb gauge. The electric field is given by $\mathbf{E} = -\partial_t \mathbf{A}$, while the magnetic induction is $\mathbf{B} = \boldsymbol{\nabla} \times \mathbf{A}$. In the case of a Gaussian pulse propagating paraxially along the positive z axis, focused cylindrically, and polarized along the x axis, the generating function is [17]

$$G_y = A_0 e^{-(\phi^2/\Delta\phi^2)-(r^2/1+z^2)} \times \cos\left[-\phi - z\frac{r^2}{1+z^2} - \mathrm{atan}(z)\right]/k_0\sqrt{1+z^2}. \quad (37)$$

Here, A_0 is the amplitude of the vector potential; $k_0 = \omega_0/c$ is the central wave number of the pulse. Space-time coordinates are normalized as follows: $r \to r/w_0$, $z \to z/z_0$, $t \to ct/z_0$, $z_0 = \frac{1}{2}k_0 w_0^2$ is the Rayleigh range, w_0 is the focal waist, $\phi = \omega_0 t - k_0 z$ is the phase, and $\Delta\phi = \omega_0 \Delta\tau$, where $\Delta\tau$ is the laser pulse duration. Using both the slow-varying envelope and the paraxial approximations, and systematically neglecting higher order terms, the 4-potential is derived. Replacing all space-time coordinates by their values along ballistic trajectories, the local 4-velocity can be evaluated by keeping terms of order A_0, $A_0\epsilon$, ϵ, and A_0^2; for example, the component parallel to the polarization, shown in Fig. 6 is

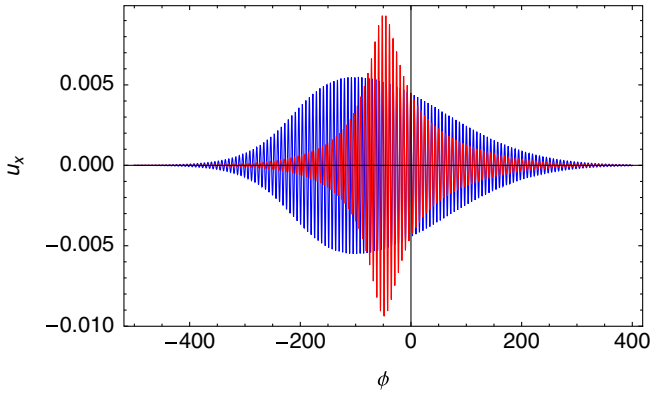

FIG. 6. Electron trajectories in the laser field for $\gamma_0 = 100$, $A_0 = 0.01$, $\Delta\phi = 200$, $x_i = y_i = 0$, $z_i = -2$, $u_{x0} = u_{y0} = 0.01$, $\epsilon = 0.01$ (blue), $\epsilon = 0.025$ (red).

$$u_x(\phi) = u_{x0} + A_0 \frac{\exp[-\frac{\phi^2}{\Delta\phi^2} - \frac{r(\phi)^2}{1+z(\phi)^2}]}{\sqrt{1+z(\phi)^2}} \times \left[1 + 4\epsilon \frac{u_{x0}}{\gamma_0 - u_{z0}} \frac{x(\phi)z(\phi)}{1+z(\phi)^2}\right] \sin[-\phi - \psi(\phi)], \tag{38}$$

where $\psi = -z[r^2/(1+z^2)] + \text{atan}(z)$.

Beyond this point, the flow of the 3D code, explained in details in Ref. [11], can be summarized as follows. All dynamical quantities are separated into slow-varying components and periodic functions; integrals over the phase are performed using the approximation: $\int f p d\phi \simeq \langle p \rangle \times \int f d\phi + f \int (p - \langle p \rangle) d\phi$, where $p(\phi + 2\pi) = p(\phi)$, and where the average is defined as $\langle p \rangle = \frac{1}{2\pi} \int_{-\pi}^{\pi} p d\phi$. For harmonic functions, $\int (p - \langle p \rangle) d\phi$ is analytical, while the integral over f can be performed efficiently because it is a slow-varying function. This approximation is used to evaluate the 4-trajectory and the radiation integral. For situations dominated by diffraction, the Fourier transform of the asymmetric Lorentzian envelope yields complex nonlinear spectra. Finally, for a $6N$-dimensional distribution of input particles in phase space, the radiation is obtained by incoherent summation; linear (blue) and nonlinear (red) spectra are shown in Fig. 9. Full 3D trajectories are used for all cases, the linear spectra are calculated from the ballistic phase $\frac{q_\mu}{\kappa}(u_0^\mu + \lambda k^\mu)\phi$ only.

IV. SOURCE DESIGN OVERVIEW

This section presents the technological design of the MEGa-ray source being currently developed at LLNL, along with the expected gamma-ray performance.

A. Accelerator systems

The accelerator begins with the radio-frequency (rf) photoinjector, based on an earlier high gradient 7 MeV, 5.5-cell X-band rf photoinjector [18]. Improvements specific to our application have been implemented. PARMELA simulations revealed that a longer first half cell, as simulated with SUPERFISH, resulted in a lower final emittance for the setup planned at LLNL. As a result, a full redesign of the rf gun has been performed using a longer first half cell, improved mode separation, a dual feed racetrack coupler, optimized coupling, and elliptical cross-section irises [19]. A schematic of the gun, low-energy beam line and a T53 (SLAC X-band linac section) is shown in Fig. 7. Superior electron beam quality, with a normalized emittance of 0.4 mm mrad (not including thermal emittance) at 250 pC charge, is ensured by the very high field applied to the photocathode: 200 MV/m, nominally. Full emittance compensation is implemented, with an optimum distance from the photocathode to the first accelerating section of 0.8 m.

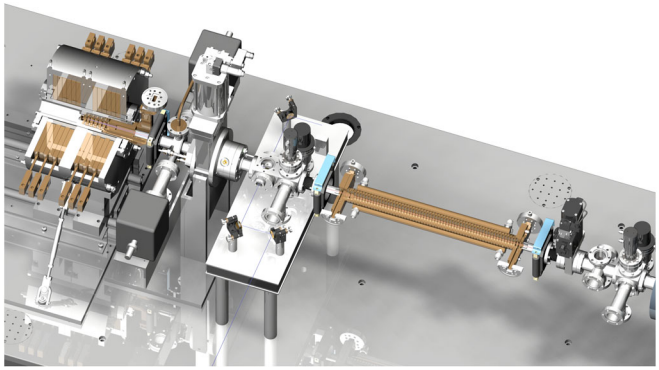

FIG. 7. Low-energy beam line, T53 section and photogun components. Full supports and rf distribution not shown.

The high power rf system is to provide adequate rf power to the accelerator to achieve the end-point electron energy. The accelerator consists of an X-band photogun and six sections of traveling wave accelerating structure comprising 53 cells, the T53VG3 (with a group velocity which is 3% of c, the speed of light). The X-band photogun is a modified version of the 5.49 cells rf gun tested at SLAC (Stanford Linear Accelerator Center) in 2002. The rf budget for the gun is 20 MW and the fill time of the structure is 65 ns. The T53VG3 type traveling wave structure was extensively tested for high gradient operation and has operated at high gradient with low breakdown rates [20]. The T-series structures are essentially the low group velocity (downstream) portion of the original 1.8 m structures [21]. This structure can be operated with extremely low trip rate at gradients up to 90 MV/m. The fill time of this structure is 74.3 ns and an rf power of 70 MW is budgeted for each section. The high power rf source is an X-band klystron (XL-4), which was developed by SLAC in the mid-1990s for the high power testing of the X-band structures. The XL-4 is a solenoid focused klystron which requires a 0.47 Tesla solenoid. The high voltage pulse required by the klystron is provided by a state-of-the-art, solid-state high voltage modulator. We have chosen the solid-state modulator (K2-3X) built by ScandiNova for its pulse-to-pulse stability and solid-state modular design; the first of these modulators has been delivered and is awaiting installation. Two klystrons and two high voltage modulators are planned for the LLNL MEGa-ray (monoenergetic gamma-ray) project. The high power pulsed rf output of two klystrons is 100 MW, 1.5 μs. The high power rf needs of the rf gun and accelerator sections are 440 MW for 210 ns (3x fill time). The logical way to achieve this is to pulse compress the output of the klystrons to 500 MW, 210 ns and to distribute the compressed pulse to the rf gun and accelerating sections. SLAC has developed and demonstrated SLED (SLAC energy doubler) II with multimode delayed lines with similar power gain factor [22]. The dual-mode SLED-II delay lines will be approximately 15 meter

long with inner diameter of 17 cm. 500 MW, 210 ns pulses are the desired output of the pulse compression system. These compressed pulses will be fed into a 13 dB coupler. The 13 dB (25 MW) output will go to the rf gun. To allow for tuning and control, a phase shifter and attenuator are put in this arm. A barrier window is also planned for the rf gun. This is to limit the number of times the rf gun is exposed to air and to possibly provide for a configuration in which the rf gun can be baked and sealed as a unit before installation. The rest of the compressed power (475 MW) is to be distributed to the linear accelerator sections. A 3 dB H-hybrid is used to divide the 475 MW in half. Then a combination of 4.8 and 3 dB H hybrids are used to distribute the power in one third portions (70 MW) to each T53 section. Phase shifters and other control elements will be added as needed.

B. Laser systems

The gamma-ray source will comprise two lasers, the interaction laser system, and the photocathode drive laser that yields the electron bunch on the photocathode. Both are seeded by the same fiber oscillator. The general architecture is similar to that presented in Ref. [6].

First the photoelectrons are generated by a 50 μJ, 263 nm spatially and temporally shaped laser pulse. The oscillator seed is amplified (using standard chirped-pulse amplification (CPA) methods) in a series of Yb-doped fiber amplifiers, beginning with standard 6-μm core pre-amps, a 29 μm core intermediate photonic crystal fiber stage, and a final 85 μm fiber rod amplifier to generate 1 mJ, 1053 nm pulses at 120 Hz that are compressed to 250 fs. These pulses are frequency quadrupled, stacked in a hyper-Michelson pulse stacker, which converts the single input pulse into eight replicas using three beam splitters; then transformed from Gaussian to a flattop transverse profile using refractive optical beam shaping components. This beam is transported to the photoinjector, resized to 1 mm, and imaged onto the cathode surface.

Second, the scattering laser should have minimal bandwidth and needs to be no shorter than 10 ps; hence, Nd:YAG with its narrow gain bandwidth is a suitable material for amplification. Because of the narrow ($<$ 1 nm) bandwidth and long ($>$ ns) desired stretched pulse length in the amplification chain, we developed a novel hyperdispersion stretcher and compressor pair [23] that provides very high ($>$ 7000 ps/nm) dispersion. The scattering laser pulse is generated by preamplifying a selected oscillator pulse in a

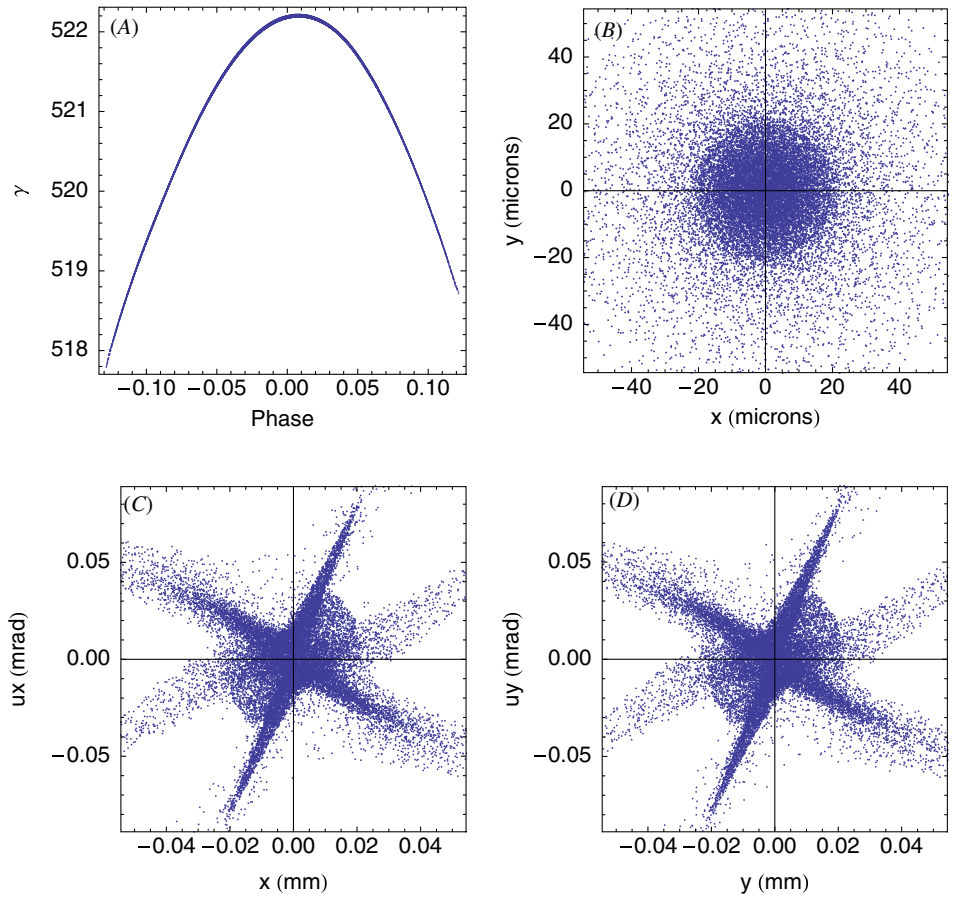

FIG. 8. PARMELA electron beam simulations: (a) γ vs radio-frequency (rf) phase, (b) beam focal spot, (c) and (d) phase space.

6 μm and 29 μm core fibers to the 30 μJ level, then doing final amplification in a set of diode-pumped Nd:YAG heads. The diode-pumping architecture allows this system to produce 1 J laser pulses at 120 Hz; subsequently compressed to 10 ps. This beam is then frequency doubled to 532 nm and transported to the interaction region.

C. Expected gamma-ray properties

By using laser and electron beam properties expected from the accelerator and laser systems described above, we have modeled the gamma-ray source properties, and, in particular, the peak brightness. Instead of using a single electron, we modeled the electron beam phase space at the interaction point by using PARMELA, as shown in Fig. 8. Then spectra from each electron of the beam are incoherently summed to yield the total spectrum from the laser/electron beam interaction. PARMELA uses macroparticles to represent the electron bunch and time steps to push particles. In our simulations, two-dimensional maps of the radio-frequency fields of the accelerator cavities were modeled with the SUPERFISH code and imported into the particle tracker. The space-charge forces are computed using a quasistatic approximation by transforming into a comoving reference frame and computing and applying the Coulomb field on a mesh. For these simulations, 20 000 macroparticles were used. This number was chosen to provide the required resolution for the Compton scattering calculation and was much greater than that required to ensure accurate modeling of the electron beam propagation through the accelerator.

The resulting gamma-ray spectrum is presented in Fig. 9, both for the linear and nonlinear case. Because of the electron beam emittance that broadens the spectrum, fine nonlinear structures cannot be seen. However, one can see that the nonlinearity of the interaction decreases the spectral brightness.

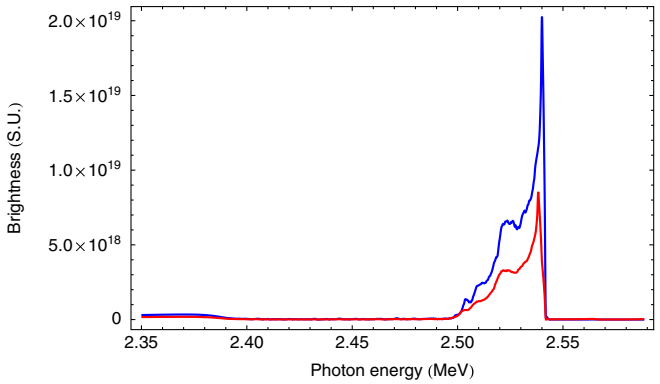

FIG. 9. Linear (blue) and nonlinear (red) spectra from the electron distribution of Fig. 8; the laser parameters are 10 ps FWHM pulse duration, 532 nm wavelength, 12 μm rms spot size, 150 mJ energy.

V. CONCLUSION AND OUTLOOK

In this paper, the design of a narrow-band Compton scattering gamma-ray source is presented within the specific context of nuclear resonance fluorescence applications. NRF is a very powerful isotope-specific process that has potential high impact applications in homeland security, nuclear waste assay and management, stockpile surveillance, or medicine. In order for this process to be fully efficient, it is necessary to operate in a spectrally narrow regime. In order to assess spectral broadening mechanisms in Compton scattering, detailed theory modeling is necessary. It is shown that two different formalisms, using the Klein-Nishina differential cross section and the classical radiation formula, yield complementary information to this problem. Indeed, recoil and nonlinear effects have to be accounted for when designing high-precision narrow-band gamma-ray sources. Challenging technological laser and accelerator designs are currently being finalized at LLNL for the design of such a new source of tunable γ rays for Department of Homeland Security and National Nuclear Security Administration missions.

ACKNOWLEDGMENTS

The authors acknowledge useful discussions with D. P. McNabb. This work was performed under the auspices of the U.S. Department of Energy by Lawrence Livermore National Laboratory under Contract No. DE-AC52-07NA27344, and supported by the U.S. Department of Homeland Security under DNDO Contract No. HSHQDC-09-X-00554/0001. We also acknowledge support from the Laboratory Directed Research and Development Program at LLNL under tracking code 09-SI-004.

[1] U. Kneissl, H. M. Pitz, and A. Zilges, Prog. Part. Nucl. Phys. **37**, 349 (1996).
[2] W. Bertozzi, J. A. Caggiano, W. K. Hensley, M. S. Johnson, S. E. Korbly, R. J. Ledoux, D. P. McNabb, E. B. Norman, W. H. Park, and G. A. Warren, Phys. Rev. C **78**, 041601(R) (2008).
[3] C. A. Hagmann, J. M. Hall, M. S. Johnson, D. P. McNabb, J. H. Kelley, C. Huibregtse, E. Kwan, G. Rusev, and A. P. Tonchev, J. Appl. Phys. **106**, 084901 (2009).
[4] N. Kikuzawa, R. Hajima, N. Nishimori, E. Minehara, T. Hayakawa, T. Shizuma, H. Toyokawa, and H. Ohgaki, Appl. Phys. Express **2**, 036502 (2009).
[5] F. Albert, S. G. Anderson, G. A. Anderson, S. M. Betts, D. G. Gibson, C. A. Hagmann, J. Hall, M. S. Johnson, M. J. Messerly, V. A. Semenov, M. Y. Shverdin, A. M. Tremaine, F. V. Hartemann, C. W. Siders, D. P. McNabb, and C. P. J. Barty, Opt. Lett. **35**, 354 (2010).
[6] D. J. Gibson, F. Albert, S. G. Anderson, S. M. Betts, M. J. Messerly, H. H. Phan, V. A. Semenov, M. Y. Shverdin,

A. M. Tremaine, F. V. Hartemann, C. W. Siders, D. P. McNabb, and C. P. J. Barty, Phys. Rev. ST Accel. Beams **13**, 070703 (2010).

[7] F. Albert, S. G. Anderson, D. J. Gibson, C. A. Hagmann, M. S. Johnson, M. Messerly, V. Semenov, M. Y. Shverdin, B. Rusnak, A. M. Tremaine, F. V. Hartemann, C. W. Siders, D. P. McNabb, and C. P. J. Barty, Phys. Rev. ST Accel. Beams **13**, 070704 (2010).

[8] W. Bertozzi, S. E. Kobly, R. J. Ledoux, and W. Park, Nucl. Instrum. Methods Phys. Res., Sect. B **261**, 331 (2007).

[9] J. Pruet, D. P. McNabb, C. A. Hagmann, F. V. Hartemann, and C. P. J. Barty, J. Appl. Phys. **99**, 123102 (2006).

[10] L. M. Brown and R. P. Feynmann, Phys. Rev. **85**, 231 (1952).

[11] F. Albert, S. G. Anderson, D. J. Gibson, R. A. Marsh, C. W. Siders, C. P. J. Barty, and F. V. Hartemann, Phys. Plasmas **18**, 013108 (2011).

[12] J. W. Meyer, Phys. Rev. D **3**, 621 (1971).

[13] F. V. Hartemann, F. Albert, C. W. Siders, and C. P. J. Barty, Phys. Rev. Lett. **105**, 130801 (2010).

[14] G. Bhatt, H. Grotch, and E Kazes, Phys. Rev. A **28**, 2195 (1983).

[15] F. V. Hartemann, A. L. Troha, N. C. Luhmann, Jr., and Z. Toffano, Phys. Rev. E **54**, 2956 (1996).

[16] http://mathworld.wolfram.com/LaguerrePolynomial.html.

[17] F. V. Hartemann, J. R. Van Meter, A. L. Troha, E. C. Landahl, N. C. Luhmann, Jr., H. A. Baldis, A. Gupta, and A. K. Kerman, Phys. Rev. E **58**, 5001 (1998).

[18] A. Vlieks *et al.*, in *High Energy Density and High Power RF: 5th Workshop*, AIP Conf. Proc. No. 625 (AIP, New York, 2002), p. 107.

[19] R. A. Marsh *et al.*, in Proceedings of the First International Particle Accelerator Conference, Kyoto, Japan (2010), THPEA056.

[20] C. Adolphsen *et al.*, in *Proceedings of the 20th Particle Accelerator Conference, Portland, OR, 2003* (IEEE, New York, 2003), pp. 668–672.

[21] G. Caryotakis, Report No. SLAC-PUB-7146, 1996.

[22] S. G. Tantawi *et al.*, Phys. Rev. ST Accel. Beams **8**, 042002 (2005).

[23] M. Y. Shverdin, F. Albert, S. G. Anderson, S. M. Betts, D. J. Gibson, M. J. Messerly, F. V. Hartemann, C. W. Siders, and C. P. J. Barty, Opt. Lett. **35**, 2478 (2010).